Aggregation Behavior of Sodium Lauryl Ether Sulfate with a Positively Bicharged Organic Salt and Effects of the Mixture on Fluorescent Properties of Conjugated Polyelectrolytes

ARTICLE *in* LANGMUIR · FEBRUARY 2015

Impact Factor: 4.46 · DOI: 10.1021/la504733q · Source: PubMed

5 AUTHORS, INCLUDING:

Yongqiang Tang
Chinese Academy of Sciences
9 PUBLICATIONS **29** CITATIONS
SEE PROFILE

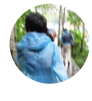

Zhang Liu
Chinese Academy of Sciences
7 PUBLICATIONS **40** CITATIONS
SEE PROFILE

Linyi Zhu
University of Oxford
12 PUBLICATIONS **68** CITATIONS
SEE PROFILE

Han Yuchun
Chinese Academy of Sciences
47 PUBLICATIONS **603** CITATIONS
SEE PROFILE

Langmuir

Article

pubs.acs.org/Langmuir

Aggregation Behavior of Sodium Lauryl Ether Sulfate with a Positively Bicharged Organic Salt and Effects of the Mixture on Fluorescent Properties of Conjugated Polyelectrolytes

Yongqiang Tang, Zhang Liu, Linyi Zhu, Yuchun Han, and Yilin Wang*

Key Laboratory of Colloid and Interface Science, Beijing National Laboratory for Molecular Sciences (BNLMS), Institute of Chemistry, Chinese Academy of Sciences, Beijing 100190, P. R. China

Supporting Information

ABSTRACT: The aggregation behavior of anionic single-chain surfactant sodium lauryl ether sulfate containing three ether groups (SLE3S) with positively bicharged organic salt 1,2-bis(2-benzylammoniumethoxy)ethane dichloride (BEO) has been investigated in aqueous solution, and the effects of the BEO/SLE3S aggregate transitions on the fluorescent properties of anionic conjugated polyelectrolyte MPS-PPV with a larger molecular weight and cationic conjugated oligoelectrolyte DAB have been evaluated. Without BEO, SLE3S does not affect the fluorescent properties of MPS-PPV and only affects the fluorescent properties of DAB at a higher SLE3S concentration. With the addition of BEO, SLE3S and BEO form gemini-like surfactant $(SLE3S)_2$-BEO. When the BEO/SLE3S molar ratio is fixed at 0.25, with increasing the BEO/SLE3S concentration, the BEO/SLE3S mixture forms large, loosely arranged aggregates and then transforms to closely packed spherical aggregates and finally to long thread-like micelles. The photoluminescence (PL) intensity of MPS-PPV varies with the morphologies of the BEO/SLE3S aggregates, while the PL intensity of DAB is almost independent of the aggregate morphologies. The results demonstrate that gemini-like surfactants formed through intermolecular interactions can effectively adjust the fluorescent properties of conjugated polyelectrolytes.

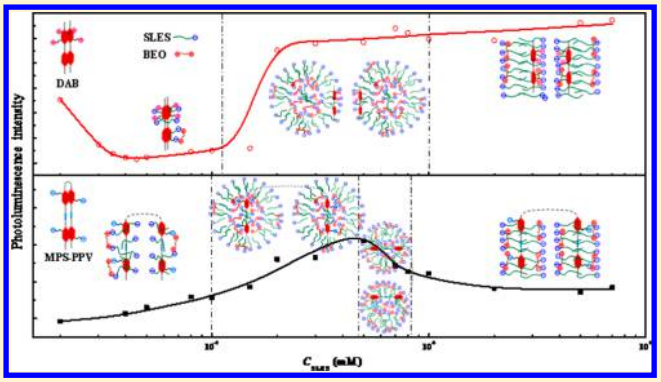

INTRODUCTION

Conjugated polyelectrolytes (CPEs) are constructed by a π-delocalized backbone with pendant ionic functionalities.[1−4] They combine the optoelectronic properties of neutral conjugated polymers and electrostatic behavior of polyelectrolytes. Comparing with neutral conjugated polymers, CPEs are soluble in polar solvents,[1,5,6] and therefore they show great promise in photovoltaic cells,[7−9] organic light-emitting diodes,[10] and biosensors.[11,12] In particular, the self-assembly of CPEs in aqueous solution leads to a red-shift of the long wavelength band and causes a reduction of photoluminescence (PL) intensity.[13,14] Moreover, surfactants can affect the aggregation behaviors of CPEs through intermolecular interactions and therefore adjust the fluorescent properties of CPEs. The effects of surfactants on the fluorescent properties strongly depend on their concentration, charge, and chain strength[5,13−20] and even on their spacer length for ionic gemini surfactants and so on.[21] The dominant intermolecular interaction of CPE molecules with nonionic or similarly charged surfactants is hydrophobic interaction. The incorporation of the hydrophobic chains of surfactants into the conjugated backbone of CPEs hinders $\pi-\pi$ stacking of the conjugated backbone and reduces the nonradiative energy transfer among the conjugated backbones, causing the PL intensity of CPEs to increase. The effects of oppositely charged surfactants on the fluorescent properties of CPEs are more complicated. It was reported that the electrostatic attraction between CPEs and the headgroups of surfactants with shorter chain induces further aggregation of CPEs and results in the decrease in PL intensity,[20] while the effect of electrostatic attraction is overcome by hydrophobic interaction with increasing the surfactant chain length and concentration, leading to the increase in PL intensity. However, most of the investigations so far focus on the effects from monomers and small micelles of surfactants. How aggregate transitions of surfactants affect the fluorescent properties of CPEs has not yet been well understood.

Gemini surfactants have very low critical micellar concentration (CMC) and very strong self-assembling ability.[22,23] Thus, they show strong ability to affect the aggregation behavior of polymers.[24,25] In principle, a gemini-like surfactant can also be constructed with two single-chain ionic surfactants and an oppositely charged organic salt by noncovalent bonds. A series of gemini-like surfactants were previously constructed with cationic single-chain surfactant cetyltrimethylammonium bromide $C_{16}H_{33}N(CH_3)_3Br$ (CTAB) and anionic dicarboxylic

Received: December 5, 2014
Revised: January 19, 2015
Published: February 1, 2015

DOI: 10.1021/la504733q
Langmuir 2015, 31, 2104−2111

acid sodiums NaOOC$(CH_2)_{n-2}$COONa (C_nNa_2, n = 4, 6, 8, 10, 12) through electrostatic attraction synchronously assisted by hydrophobic interaction.[26] It was also shown that a gemini-like surfactant was constructed by sodium dodecyl sulfate (SDS) and 1,2-bis(2-benzylammoniumethoxy)ethane dichloride (BEO) predominantly through electrostatic attraction as well as hydrophobic interaction and $\pi-\pi$ interaction.[27] The SDS/BEO mixture forms large loose irregular aggregates, spherical vesicles, and then long thread-like micelles with the increase of SDS concentration. This mixture with diverse aggregate morphologies should be a proper system to be used to investigate the effects of aggregate transitions on the fluorescent properties of CPEs. However, precipitation is caused by charge neutralization at a wider mixing ratio range. Choosing appropriate surfactants and connecting organic salts with more hydrophilic groups may be a feasible method to avoid precipitation. Sodium lauryl ether sulfate (SLES) contains ether groups and has a larger solubility in water than SDS. Moreover, compared with SDS, SLES is milder,[28−31] more easily biodegraded,[32−34] less prone to precipitation in high ionic strength medium,[35] and has lower CMC and higher surface activity.[36−38] So SLES is a good candidate to construct a gemini-like surfactant with BEO to avoid precipitation.

In this work, single-chain surfactant sodium lauryl ether sulfate with three ether groups (SLE3S) and positively bicharged organic salt BEO are chosen to construct a gemini-like surfactant, and the BEO/SLE3S aggregates are used to manipulate the fluorescence properties of two conjugated polyelectrolytes (CPEs): poly[2-methoxy-5-propyloxysulfonate phenylenevinylene] (MPS-PPV) with a larger molecular weight and poly[(2,5-bis(2-(*N*,*N*-diethylammonium bromide)ethoxy)-1,4-phenylene)-*alt*-1,4-phenylene] (DAB) with a smaller molecular weight. The results show that a gemini-like surfactant $(SLE3S)_2$-BEO is formed, and the BEO/SLE3S mixture forms large, loosely arranged aggregates, closely packed spherical aggregates, and long thread-like micelles by adjusting the mixing ratio and concentration. In particular, the effects of the BEO/SLE3S aggregates on the fluorescent properties of CPEs are closely related to the aggregate size and morphology, and the charge property at the aggregate/solution interface. This work provides a way to apply the different aggregates of gemini-like surfactants formed through intermolecular interactions to manipulate the fluorescence properties of CPEs.

EXPERIMENTAL SECTION

Materials. Sodium lauryl ether sulfate (SLE3S) was purchased from Langchem Inc. (Shanghai, China). The raw SLE3S was first dissolved in ethanol at about 60 °C and then filtered while hot to remove solid impurities. Recrystallizing the residue three times from ethanol gave a white, crystalline product. 1,2-Bis(2-benzylammoniumethoxy)ethane dichloride (BEO) was synthesized through neutralizing 1,2-bis(2-benzylaminoethoxy)ethane (>90%, TCI, Japan) with hydrochloric acid in ethanol and purified by recrystallizing with ethanol for three times as described by Yu et al.[27] The purity of the obtained BEO was characterized by ^{1}H NMR and elemental analysis. MPS-PPV (M_w = (1.2−2.0) × 10^7 g/mol) and DAB (M_w = 1054 g/mol) were purchased from Sigma-Aldrich Co., Ltd., and used without further purification. The concentrations of MPS-PPV and DAB were fixed at 40 μM in repeat units. Deionized water (18.2 MΩ·cm) from Milli-Q equipment were used throughout.

Surface Tension Measurements. Surface tension measurements of BEO/SLE3S mixed solution were carried out by the drop volume method. Each surface tension value was determined from at least five consistent measured values. Each surface tension curve was repeated three times. The measurement temperature was controlled at 25.00 ± 0.05 °C. The standard error of the surface tension data was 1 mN/m.

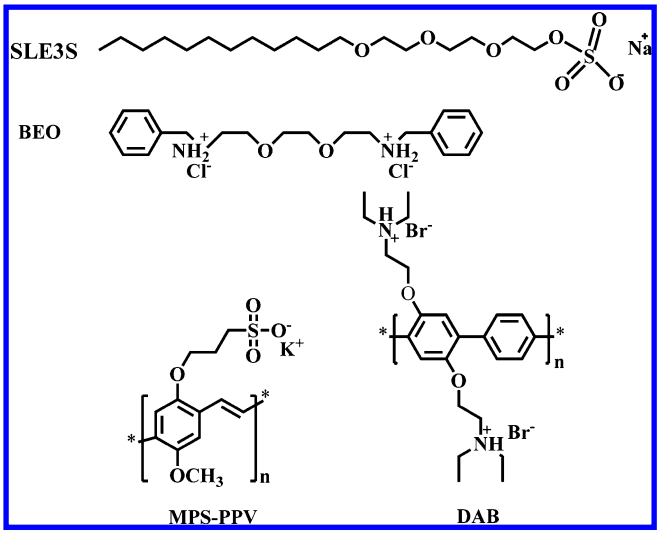

Figure 1. Chemical structures of SLE3S, BEO, MPS-PPV, and DAB.

Isothermal Titration Microcalorimetry (ITC). The ITC experiment was taken in a TAM 2277-201 microcalorimetric system (Thermometric AB, Järfälla, Sweden) with a stainless steel sample cell of 1 mL at 25.00 ± 0.01 °C. The BEO solution was titrated into the SLE3S solution via a 500 μL Hamilton syringe controlled by a 612 Thermometric Lund pump until the desired range of concentration had been covered. Each ITC curve was repeated at least twice with deviation within 5%.

ζ-Potential Measurements. ζ-Potential measurements were carried out with a Nano-ZS instrument (ZEN3600, Malvern Instruments, Worcestershire, U.K.) equipped with a thermostated chamber and employing a 4 mW He−Ne laser (λ = 632.8 nm) at 25.00 ± 0.01 °C. The ζ-potential measurement of each sample was repeated for three times, and the average value was taken.

Turbidity Measurements. Turbidity measurements were used to monitor the molar ratio dependence and the concentration dependence of the BEO/SLE3S mixed aggregates. The turbidity of the BEO/SLE3S mixed solutions at different BEO/SLE3S molar ratio, expressed by 100 − %T, was measured at 450 nm using a Brinkman PC920 probe colorimeter thermostated at 25.0 ± 0.1 °C. The measurements were corrected by taking the turbidity of Milli-Q water as zero.

Dynamic Light Scattering (DLS). DLS measurements were carried out by an LLS spectrometer (ALV/SP-125) with a multi-τ digital time correlator (ALV-5000) at 25.0 ± 0.1 °C. A solid-state He−Ne laser (output power of 22 mW at λ = 632.8 nm) was used as a light source, and all the measurements for the BEO/SLE3S mixtures were conducted at a scattering angle of 90°. The samples were filtered through a 0.45 μm PVDF membrane filter (Millipore). The correlation function of the scattering data was analyzed via the CONTIN method to obtain the distribution of diffusion coefficients (D) of the aggregates, and then the apparent equivalent hydrodynamic radius (R_h) was determined using the Stokes−Einstein equation $R_h = kT/6\pi\eta D$, where k is the Boltzmann constant, T is the absolute temperature, and η is the solvent viscosity. The relative errors of aggregate sizes are within 3%.

UV−Vis and Fluorescence Spectra. The spectra of BEO/SLE3S/MPS-PPV and BEO/SLE3S/DAB were recorded within 1−2 min of the sample preparation at 25 °C. The absorption spectra were recorded in quartz cuvettes (path length 1 cm) by a SHIMADZU UV 1601PC spectrometer, while fluorescence spectra were measured in a quartz cell (1 cm × 1 cm) with both the excitation and emission slits of 10 nm width by a Hitachi model F-4500 spectrofluorometer. The excitation wavelengths of MPS-PPV and DAB were fixed at 450.0 and 330.0 nm, respectively. The PL intensity is taken from the emission maxima of the fluorescence emission spectra.

DOI: 10.1021/la504733q
Langmuir 2015, 31, 2104−2111

RESULTS AND DISCUSSION

Formation of Gemini-like Surfactant. First the properties and aggregation behavior of the BEO/SLE3S mixture have been studied.

Surface tension curves of the BEO/SLE3S solutions at different BEO/SLE3S molar ratios ($R_{BEO/SLE3S}$) are shown in Figure 2. Because BEO has almost no surface activity, the

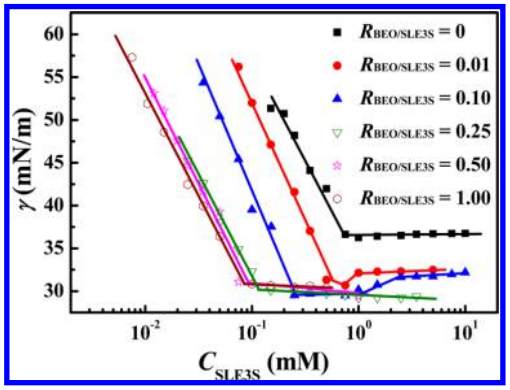

Figure 2. Surface tension (γ) plotted against SLE3S concentration (C_{SLE3S}) at different $R_{BEO/SLE3S}$ (25.0 °C).

abscissa of Figure 2 is expressed as the SLE3S concentration (C_{SLE3S}) rather than the total concentration of SLE3S and BEO. The values of the critical micellar concentration (CMC), the surface tension at CMC (γ_{CMC}), and the surfactant concentration required to reduce the surface tension of water by 20 mN/m (C_{20}) are derived from the surface tension curves and listed in Table 1. Obviously, the addition of BEO significantly

Table 1. CMC, γ_{CMC}, and C_{20} of the BEO/SLE3S Solutions at Different $R_{BEO/SLE3S}$ and 25 °C

$R_{BEO/SLE3S}$	0	0.01	0.10	0.25	0.50	1.00
CMC (mM)	0.75	0.54	0.26	0.12	0.086	0.091
γ_{CMC} (mN/m)	36.7	32.1	29.6	30.2	30.9	30.8
C_{20} (mM)	0.17	0.10	0.04	0.01	0.01	0.01

reduces the values of CMC, γ_{CMC} and C_{20}. The mixture of BEO and SLE3S has much higher surface activity and stronger aggregation ability than SLE3S itself. For SLE3S without BEO, the surface tension curve shows a breakpoint at C_{SLE3S} = 0.75 mM, which is the CMC of SLE3S.[38] With the increase of the $R_{BEO/SLE3S}$, the CMC value decreases. In particular, at $R_{BEO/SLE3S}$ = 0.01 and 0.10, beside the CMC of the BEO/SLE3S mixture, the surface tension curves show an arising process near the CMC of SLE3S. When $R_{BEO/SLE3S}$ is beyond 0.25, each of the surface tension curves shows only one inflection point, i.e., CMC, just like most single-component surfactants. Moreover, further increasing $R_{BEO/SLE3S}$ only slightly reduces the CMC. The CMC values and the surface tension curves at $R_{BEO/SLE3S}$ = 0.50 and 1.00 coincide with each other. This suggests that the binding of BEO with SLE3S reaches a saturation when $R_{BEO/SLE3S}$ is between 0.25 and 0.50. The existence of the two transition points for the surface tension curves at lower $R_{BEO/SLE3S}$ may be caused by the coexistence of the BEO/SLE3S complexes and unbound SLE3S molecules.

In order to understand the binding between SLE3S and BEO, the ITC experiment was performed by titrating 0.40 mM BEO solution into 0.070 mM SLE3S solution. The observed enthalpies (ΔH_{obs}) are plotted against $R_{BEO/SLE3S}$ in Figure 3. With the addition of BEO, the ITC curve experiences a process

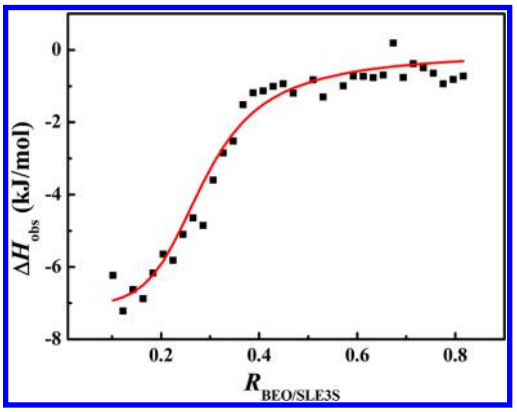

Figure 3. ITC data and thermodynamic fitting curve as a function of $R_{BEO/SLE3S}$ for the binding of BEO with SLE3S at 25.0 °C.

from large exothermic value to near zero. The large exothermic enthalpy indicates that BEO binds with SLE3S through strong electrostatic binding. The binding ratio of BEO to SLE3S can be calculated by fitting the ITC curve with the Digitam 4.1 software from Thermometric AB. The obtained binding number of BEO molecules per SLE3S molecule is about 0.40. This confirms that one BEO molecule binds to about two SLE3S molecules and forms gemini-like surfactant $(SLE3S)_2$-BEO. The positively charged organic salt BEO acts as a spacer.

Aggregate Transitions. As stated above, the BEO molecules bind with the SLE3S molecules and form gemini-like surfactant $(SLE3S)_2$-BEO. This structure significantly affects the surface activity and CMC in the mixture. Because the surface tension curves at $R_{BEO/SLE3S}$ = 0.25, 0.50, and 1.0 are very close to each other, it is suggested that the aggregation behaviors of the BEO/SLE3S mixture are similar at these three mixing molar ratios. Similar to the BEO/SDS mixture, the BEO/SLE3S mixture was also precipitated when the molar ratio was close to 0.5. But the precipitation of the BEO/SLES mixture was much slower than the BEO/SDS mixture, and the BEO/SLE3S precipitates could be dissolved with a less amount of surfactant. Therefore, in the following section, the BEO/SLE3S mixture at $R_{BEO/SLE3S}$ = 0.25 is chosen as a representative to study the aggregation behavior of the $(SLE3S)_2$-BEO structure in aqueous solution.

The turbidity of the BEO/SLE3S mixed solution and the size distribution of the aggregates with increasing the total concentration of BEO and SLE3S are studied and are shown against the SLE3S concentration (C_{SLE3S}) in Figure 4. In the surfactant concentration range studied, the aggregates are all soluble without precipitation. Figure 4a shows that the turbidity rises significantly beyond 0.10 mM, which is near the CMC value at $R_{BEO/SLE3S}$ = 0.25 determined from the surface tension curve. Then the turbidity increases to a maximum at ~0.50 mM and decreases after the maximum. Beyond 1.00 mM, the decrease of turbidity becomes tardily, and the turbidity comes back to zero again at higher concentration. Figure 4b indicates that the aggregates at C_{SLE3S} = 0.20 and 0.70 mM, which are located at both sides of the turbidity maximum, are large aggregates with a hydrodynamic radius R_h of ~150 nm. The large aggregates change into small aggregates of R_h ~ 30 nm at C_{SLE3S} = 1.0 mM. While further increasing C_{SLE3S} to 5.0 mM, the aggregates present two size distributions: one is at R_h = 2−3

DOI: 10.1021/la504733q
Langmuir 2015, 31, 2104−2111

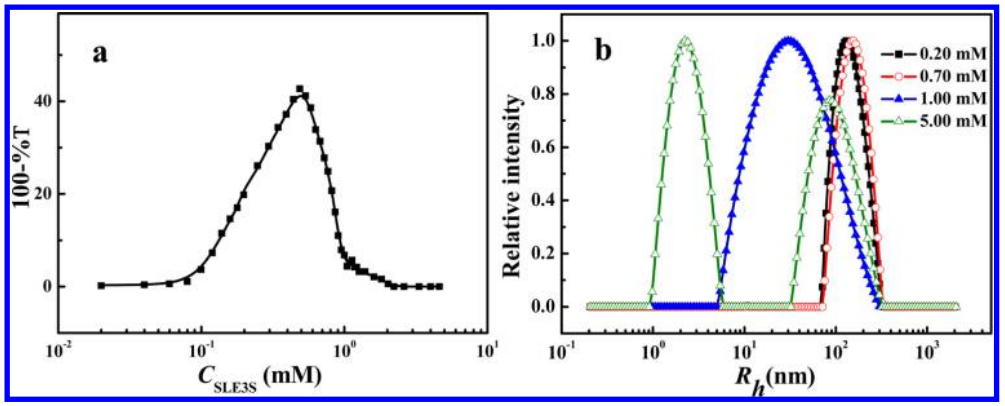

Figure 4. Turbidity (a) and size distribution (b) with increasing the SLE3S concentration C_{SLE3S} at $R_{BEO/SLE3S}$ = 0.25 (25.0 °C).

nm, and another is at $R_h \sim 80$ nm. The relative intensity of the larger one is much weaker than that of the small one.

The cryo-TEM images of the aggregates at the corresponding C_{SLE3S} above are shown in Figure 5. At C_{SLE3S} = 0.20 mM

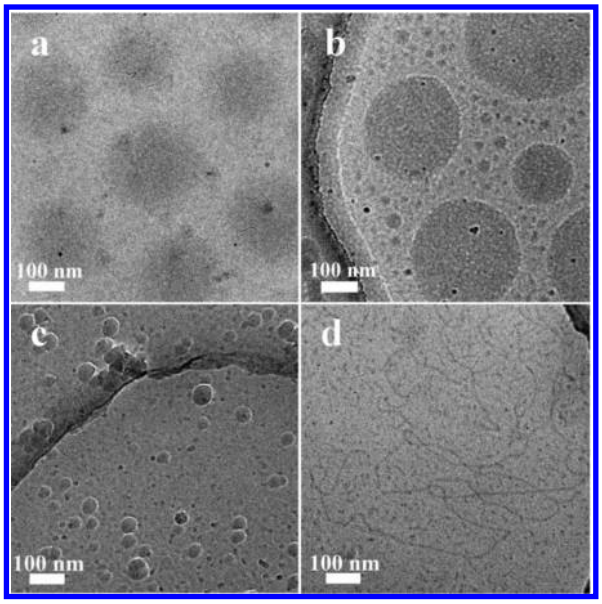

Figure 5. Cryo-TEM images of the BEO/SLE3S mixed solutions at $R_{BEO/SLE3S}$ = 0.25 and different SLE3S concentrations: (a) 0.20, (b) 0.70, (c) 1.0, and (d) 5.0 mM.

(Figure 5a), the aggregates are large, loosely arranged spherical aggregates. At C_{SLE3S} = 0.70 mM (Figure 5b), the aggregates are closely packed spherical aggregates. Then at C_{SLE3S} = 1.00 mM, the aggregates become compact spherical aggregates with a diameter smaller than 100 nm (Figure 5c). At C_{SLE3S} = 5.00 mM, the aggregates are long thread-like micelles with a small amount of very small spherical micelles (Figure 5d). The aggregate transitions are consistent with the results from turbidity and DLS. That is to say, the aggregates exhibit remarkable changes with increasing the SLE3S concentration while fixing the molar ratio of BEO to SLE3S. Below the CMC of the BEO/SLE3S mixture, all of the BEO and SLE3S molecules exist as monomers or the $(SLE3S)_2$-BEO complexes. When the SLE3S concentration exceeds CMC, loosely arranged spherical aggregates are formed. The structure of the loosely arranged spherical aggregates should be similar to that we proposed in the BEO/SDS system.[27] Each BEO molecule may bind with two SLE3S molecules through electrostatic interaction as proved above, being assisted by the hydrophobic interaction between the alkyl chains of SLE3S and BEO and the $\pi-\pi$ interaction between the benzene rings of BEO. Thus, the BEO/SLE3S mixed solution mainly contains two kinds of surfactant structures, gemini-like surfactant $(SLE3S)_2$-BEO and excessive single-chain surfactant SLE3S. With increasing C_{SLE3S}, the hydrophobic interaction is enhanced gradually. Above 0.5 mM, the hydrophobic interaction becomes strong enough; therefore, the loosely arranged spherical aggregates transform to closely packed spherical aggregates. Beyond 1.0 mM, the gradually enhanced hydrophobic interaction between the SLE3S hydrophobic chains makes the SLE3S molecules pack more tightly in the aggregates, so closely packed spherical aggregates transform into thread-like micelles.

Effects of Aggregate Transitions on Fluorescence Properties of CPEs. In the following text, the different BEO/SLE3S aggregates at $R_{BEO/SLE3S}$ = 0.25 revealed above are chosen to study their influences on the fluorescence properties of negatively charged MPS-PPV and positively charged DAB. The concentrations of MPS-PPV and DAB are both fixed at 0.040 mM in repeat units. Figure 6 shows the variations of the UV absorbance, photoluminescence intensity (PL), and ζ-potential of the BEO/SLE3S mixed aggregates with MPS-PPV and DAB against C_{SLE3S}. Apparently, the BEO/SLE3S aggregates show different effects on the photoluminescence properties of MPS-PPV and DAB. Of particular, these effects strongly depend on if BEO is added. Moreover, the critical points for the variations of the UV absorbance, photoluminescence intensity (PL), and ζ-potential are closely related with each other. In order to describe the curves conveniently, these critical points are marked in the figures. Considering the structure, size, and charge of the BEO/SLE3S aggregates and the critical concentrations for the aggregate transitions revealed in the former text, the effects on the fluorescent properties of negatively charged MPS-PPV and positively charged DAB can be understood with the simplified models in Figure 7. The detail discussion will be presented in the following text.

The effects of the BEO/SLE3S aggregates at $R_{BEO/SLE3S}$ = 0.25 on the fluorescent properties of MPS-PPV are shown in the left of Figure 6 (Figure 6a–c). The characteristic absorption peaks of MPS-PPV are obscure in the surfactant concentration range studied (Figure S1). The addition of the BEO/SLE3S mixture to the aqueous dispersion of MPS-PPV leads to a blue-shift in UV absorbance when the SLE3S concentration (C_{SLE3S}) is below C_1 but a red-shift beyond C_3. Between C_1 and C_3, the

DOI: 10.1021/la504733q
Langmuir 2015, 31, 2104–2111

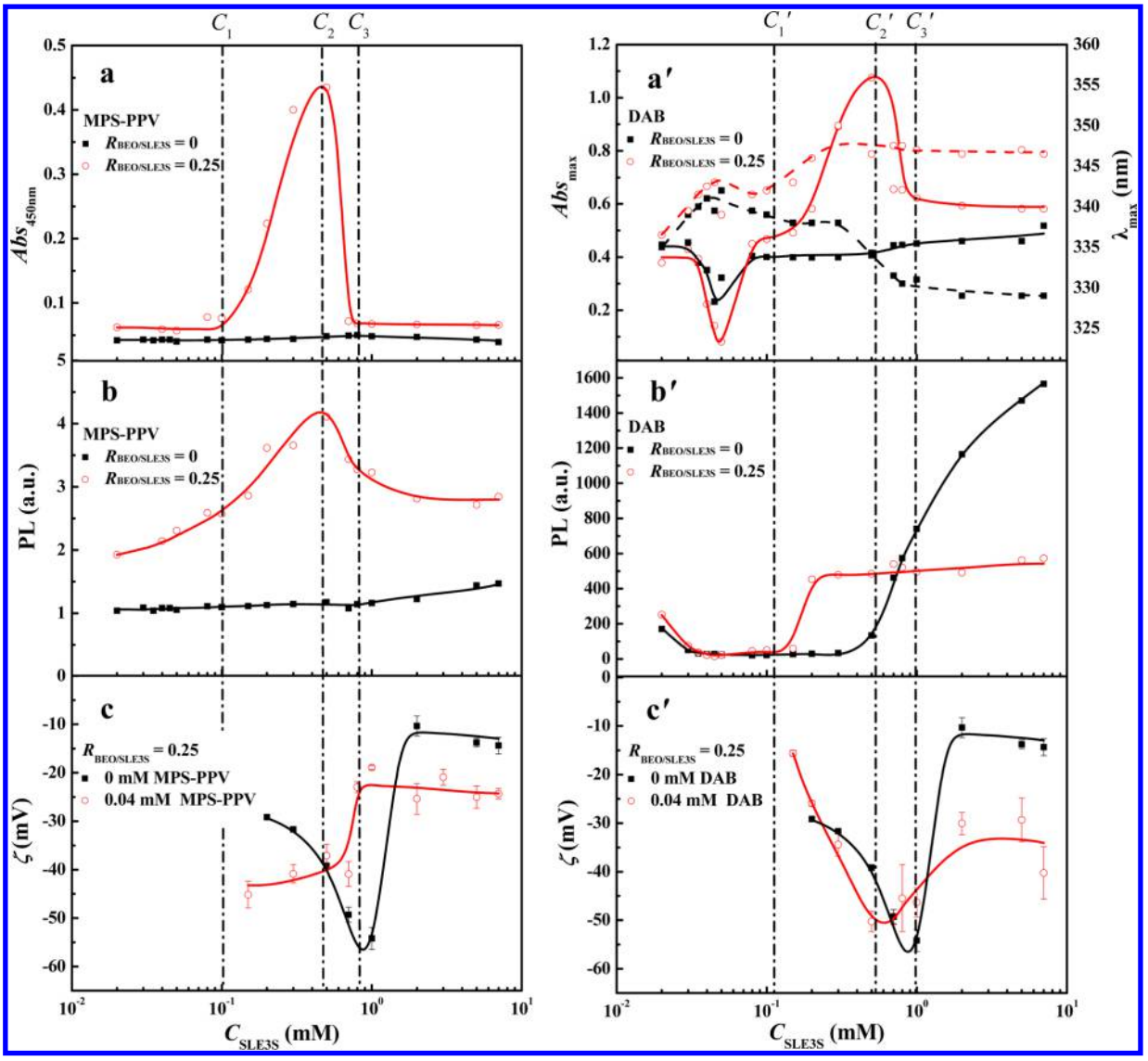

Figure 6. UV absorbance of MPS-PPV at 450 nm (a), the maximum absorbance (full line) and the maximum absorbance wavelength of DAB (dotted line) (a′), and the fluorescence intensity of MPS-PPV (b) and DAB (b′) with and without the BEO/SLE3S aggregates. The ζ-potential values of the BEO/SLE3S aggregate itself and the BEO/SLE3S aggregate with MPS-PPV (c) and DAB (c′). The temperature for all the experiments is at 25.0 °C. $R_{BEO/SLE3S}$ = 0 (square) and 0.25 (circle).

absorption peak is concealed due to the high turbidity of the mixed solution. Therefore, the UV absorbance of MPS-PPV at 450 nm, which is the maximum absorbance wavelength of MPS-PPV without any additives, is used to monitor the effect of the BEO/SLE3S aggregates on MPS-PPV.

Without BEO, SLE3S does not affect the UV absorbance and PL intensity of MPS-PPV (Figure 6a,b). The CMC of SLE3S is about 0.75 mM, and SLE3S forms small micelles above the CMC. When only anionic SLE3S is added into anionic conjugated MPS-PPV, the SLE3S molecules exist as monomers below the CMC. The SLE3S monomers can interact with MPS-PPV through hydrophobic interaction. Above the CMC, the conjugated backbone of MPS-PPV can be located in the SLE3S small micelles, and the electrostatic repulsion and steric hindrance between the micelles may prevent the $\pi-\pi$ stacking of the conjugated backbone of MPS-PPV. However, in both of the cases, the influences on MPS-PPV from the monomers and small micelles of SLE3S are very weak because SLE3S carries the same charge property as MPS-PPV. Therefore, SLE3S itself does not affect the UV absorbance and PL intensity of MPS-PPV.

Differently, if cationic BEO is added together with SLE3S, the UV absorbance and PL intensity of MPS-PPV vary significantly with the increase of BEO/SLE3S concentration. Both the UV absorbance and PL intensity of MPS-PPV display a similar variation tendency: keeping a constant or slowly increasing before C_1, reaching a maximum at C_2, then decreasing dramatically, and finally becoming a constant or a low value beyond C_3. The ζ-potential values of the BEO/SLE3S/MPS-PPV mixed aggregates (Figure 6c) indicate that the aggregates is highly negatively charged below C_2, but the negative surface charge density of the aggregates decreases steeply beyond C_2 and stops to decrease above C_3. The ζ-potential values of the BEO/SLE3S mixed aggregates in the absence of MPS-PPV also display the similar transition regions, but the values are larger than those of the BEO/SLE3S/MPS-PPV mixed aggregates before C_2 and beyond C_3, but much smaller between C_2 and C_3. As proved above, the BEO/SLE3S

DOI: 10.1021/la504733q
Langmuir 2015, 31, 2104−2111

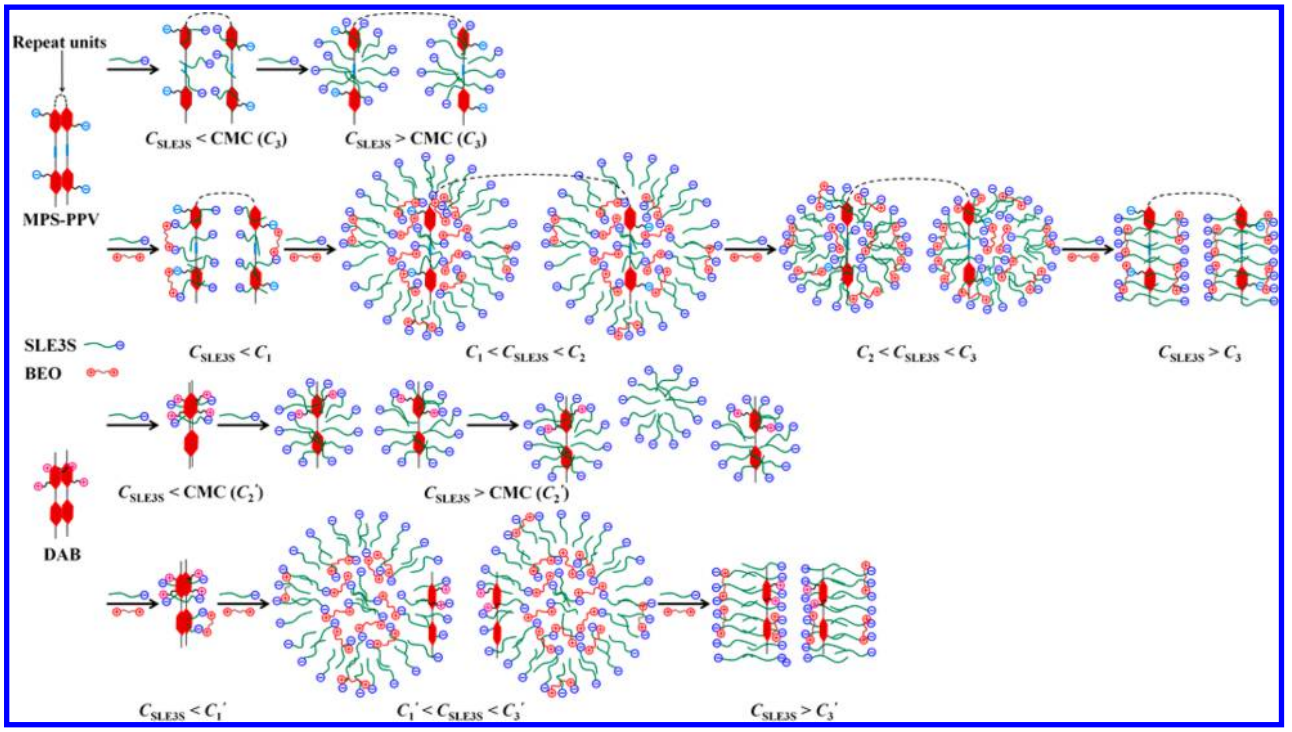

Figure 7. Proposed models for the interactions of the SLE3S and BEO/SLE3S aggregates with MPS-PPV and DAB.

mixture forms loosely large aggregates beyond the CMC of the mixture, i.e., 0.12 mM SLE3S, changes to closely packed spherical aggregates beyond 0.5 mM SLE3S, and then transfers into long thread-like micelles above 1.0 mM SLE3S. Coincidently, these three transition points for the BEO/SLE3S aggregate structures are respectively consistent with the three critical points (C_1, C_2, and C_3) for the changes of the UV absorbance and PL intensity of MPS-PPV. This means that the aggregate structures and charge properties determine the UV absorbance and PL intensity of MPS-PPV. Before C_1, i.e., the CMC of the BEO/SLE3S mixture, the hydrophobic interaction SLE3S with MPS-PPV is still very weak and not enough to change the UV absorbance of MPS-PPV. However, the PL intensity of MPS-PPV is enhanced upon the addition of the BEO/SLE3S mixture because the electrostatic attraction between cationic BEO and anionic MPS-PPV helps to the interaction and penetration of SLE3S with MPS-PPV, which weakening the $\pi-\pi$ stacking between the conjugated groups of MPS-PPV to some extent. Between C_1 and C_2, the MPS-PPV is distributed in the large, loosely packed, negatively charged aggregates formed by $(SLE3S)_2$-BEO through the hydrophobic interaction of MPS-PPV with the hydrophobic domain of the BSO/SLE3S aggregates and electrostatic attraction between anionic MPS-PPV and cationic BEO. The large aggregates produce pronounced steric hindrance between the conjugated groups of MPS-PPV. This situation effectively inhibits the $\pi-\pi$ stacking of the conjugated backbone of MPS-PPV and in turn reduces the nonradiative energy transfer among the conjugated backbones; therefore, the UV absorbance and PL intensity of MPS-PPV increase markedly. Above C_2, the BEO/SLE3S aggregates transfer to closely packed spherical aggregates with a larger negative charge density and smaller size; however, the involvement of MPS-PPV makes the BEO/SLE3S/MPS-PPV mixed aggregates carry lower negative charge density, possible because MPS-PPV promotes the transition of the mixed aggregates from high charge density to low charge density or make more BEO be bound at the aggregate surface. The weakened negative charge density decreases the electrostatic repulsion among the aggregates. Moreover the aggregates are smaller than those before C_2. So these factors reduce the steric hindrance between conjugated backbones of MPS-PPV. As a result, the UV absorbance and PL intensity start to reduce continuously. Beyond C_3, the spherical aggregates of BEO/SLE3S transform into threadlike micelles, and the charge density of the mixed aggregates is smaller and nearly does not change anymore. The thin threadlike micelles cannot effectively inhibit the $\pi-\pi$ stacking of the conjugated backbone of MPS-PPV. Thus, the PL intensity of MPS-PPV is very low in the aggregates. Subsequently, the PL intensity keeps almost unchanged because the BEO/SLE3S aggregates do not change anymore.

Compared with the effects of the BEO/SLE3S aggregates on the fluorescent properties of MPS-PPV described above, the influences of the BEO/SLE3S aggregates on DAB exhibit a more complicated changing process as shown in Figure 6a′−c′. All the UV spectra show characteristic absorbance peaks, so the variations of both the maximum absorbance value and maximum absorbance wavelength are presented (Figure 6a′). The intermolecular interactions of DAB with BEO/SLE3S are different from those of MPS-PPV with BEO/SLE3S. There are strong electrostatic binding between positively charged DAB and negatively charged SLE3S.

Before C_1', all the UV absorbance and the PL intensity for DAB are similar no matter whether BEO exists: showing a minimum in the maximum absorbance value, presenting a maximum in the maximum absorption wavelength of DAB, and the PL intensity of DAB decreasing and then becoming a very low constant value close to zero. Because the C_1' value is far lower than the CMC of SLE3S itself, but just corresponds to the CMC of the BEO/SLE3S mixture at $R_{BEO/SLE3S} = 0.25$, the interaction mainly takes place between DAB and the SLE3S monomers or the $(SLE3S)_2$-BEO complexes through electro-

DOI: 10.1021/la504733q
Langmuir 2015, 31, 2104−2111

static binding before C_1'. The strong electrostatic binding cannot obviously change the $\pi-\pi$ stacking state of DAB, but slightly induces precipitation, which causes the minimum in the UV absorbance due to the sedimentation of the precipitate.

Beyond C_1', all the results for the DAB system strongly rely on the addition of BEO. Without BEO, the UV absorbance value almost does not change anymore beyond C_1', while the maximum absorption wavelength blue-shifts to a low value and stops to change beyond C_3'. Meanwhile, the PL intensity of DAB with SLE3S rises significantly since C_2', which is slightly lower than the CMC of SLE3S. In this period, more anionic SLE3S molecules bind with cationic DAB by electrostatic interaction, and the interaction can promote the micellization of SLE3S. Therefore, DAB are dissolved in the small SLE3S micelles through hydrophobic interaction beyond C_2'. As a result, the UV absorption wavelength of DAB blue-shifts. With adding more and more small SLE3S micelles, the PL intensity is increasing significantly because the DAB dissolved in the micelles may be separated from each other to a great extent by the free micelles.

In the presence of BEO, the maximum absorption wavelength starts to red-shift above C_1' and no longer changes beyond C_2', whereas the maximum absorbance value starts to increase since C_1' and displays a remarkable maximum at C_2' and later nearly keeps a constant beyond C_3'. In another aspect, the PL intensity of DAB with the BEO/SLE3S mixture is enhanced since C_1' and then quickly becomes a constant. The variations of the ζ-potential of the BEO/SLE3S/DAB aggregates also show transition points at C_2' and C_3'. The smaller negative ζ-potential quickly becomes larger since C_1' and then reaches a negative maximum at C_2', and above C_3', the negative ζ-potential value is almost a constant. The three critical points for the BEO/SLE3S/DAB system also match the transition points of the BEO/SLE3S aggregates. Because C_1' corresponds to the CMC of BEO/SLE3S and the BEO/SLE3S mixture forms larger aggregates between C_1' and C_2', more anionic SLE3S molecules bind with cationic DAB by electrostatic interaction, and DAB molecules are dissolved in the large BEO/SLE3S aggregates through hydrophobic interaction in this period. As a result, the UV absorbance and the PL intensity increase significantly, and the UV absorption wavelength of DAB red-shifts. As a conjugated polyelectrolyte, DAB molecules without additives cannot exhibit a perfect coplanar conformation due to the electrostatic repulsion between their positively charged groups. The electrostatic neutralization of DAB by SLE3S may flatten the twisted DAB backbone, which may induce the red-shift of the absorption wavelength. The solubilization of DAB in the large BEO/SLE3S aggregates hinders the $\pi-\pi$ stacking between the conjugated backbones, resulting in the increase of the PL intensity beyond C_1'. It is noted that the absorption wavelength of DAB further red-shifts since C_1', which indicates that DAB locates in a polar environment. Considering that the PL intensity does not change with the structure transition of the BEO/SLE3S aggregates at higher concentration, the DAB molecules should be located at the aggregate/water interface mainly controlled by the electrostatic binding between the cationic charges of DAB and the anionic charges of the SLE3S headgroups. Therefore, the $\pi-\pi$ stacking of DAB is independent of the aggregate size, leading to the constant PL intensity after its initial increasing. Moreover, this location of DAB may facilitate the $\pi-\pi$ stacking of DAB, so the PL intensity of DAB in the BEO/SLE3S mixed solution is lower than that in pure water.

CONCLUSIONS

This work investigated the aggregation behavior of single-chain anionic surfactant SLE3S with positively bicharged organic salt BEO and the effects of the BEO/SLE3S aggregate transitions on the fluorescent properties of anionic conjugated polyelectrolyte MPS-PPV and cationic conjugated oligoelectrolyte DAB. It is verified that BEO and SLE3S form gemini-like surfactant $(SLE3S)_2$-BEO taking BEO as a spacer, and the gemini-like surfactant forms large, loosely arranged spherical aggregate, closely packed spherical aggregate, and long thread-like micelles with increasing the BEO/SLE3S concentration while fixing the BEO/SLE3S mixing molar ratio at 0.25. These aggregate transitions significantly affect the fluorescent properties of MPS-PPV and DAB, and the situations are different between MPS-PPV and DAB. The resulting PL intensity of the conjugated polyelectrolytes in the aggreagtes mainly depends on the size and surface charge of aggregates and the location of the conjugated polyelectrolytes in the aggregates. In particular, BEO plays an important role in adjusting the fluorescent properties of conjugated polyelectrolytes. This work sheds new light on how surfactant aggregate structures affect the fluorescent properties of conjugated polyelectrolytes. This work also provides a convenient approach to adjust the fluorescent properties of conjugated polyelectrolytes through forming gemini-like surfactant by adding a bicharged organic ion into a traditional single-chain surfactant. This approach can effectively adjust the fluorescent properties of both cationic and anionic conjugated polyelectrolytes by using the same surfactant.

ASSOCIATED CONTENT

Supporting Information

UV absorbance spectra of MPS-PPV in the presence of BEO/SLE3S mixture. This material is available free of charge via the Internet at http://pubs.acs.org.

AUTHOR INFORMATION

Corresponding Author

*E-mail: yilinwang@iccas.ac.cn (Y.W.).

Notes

The authors declare no competing financial interest.

ACKNOWLEDGMENTS

We are grateful for financial support from National Natural Science Foundation of China (Grants 21025313 and 21321063).

REFERENCES

(1) Jiang, H.; Taranekar, P.; Reynolds, J. R.; Schanze, K. S. Conjugated Polyelectrolytes: Synthesis, Photophysics, and Applications. *Angew. Chem., Int. Ed.* **2009**, *48*, 4300−4316.

(2) Marques, A. T.; Pinto, S. M. A.; Monteiro, C. J. P.; Melo, J. S. S.; Burrows, H. D.; Scherf, U.; Calvete, M. J. F.; Pereira, M. M. Energy Transfer from Fluorene-Based Conjugated Polyelectrolytes to On-Chain and Self-Assembled Porphyrin Units. *J. Polym. Sci., Part A: Polym. Chem.* **2012**, *50*, 1408−1417.

(3) Lavigne, J. J.; Broughton, D. L.; Wilson, J. N.; Erdogan, B.; Bunz, U. H. F. "Surfactochromic" Conjugated Polymers: Surfactant Effects on Sugar-Substituted PPEs. *Macromolecules* **2003**, *36*, 7409−7412.

DOI: 10.1021/la504733q
Langmuir 2015, 31, 2104−2111

(4) Heeley, M. E. H.; Gallaher, J. K.; Nguyen, T. L.; Woo, H. Y.; Hodgkiss, J. M. Surfactant Controlled Aggregation of Conjugated Polyelectrolytes. *Chem. Commun.* **2013**, *49*, 4235−4237.
(5) Henson, Z. B.; Zhang, Y.; Nguyen, T. Q.; Seo, J. H.; Bazan, G. C. Synthesis and Properties of Two Cationic Narrow Band Gap Conjugated Polyelectrolytes. *J. Am. Chem. Soc.* **2013**, *135*, 4163−4166.
(6) Lee, K.; Kim, H. J.; Kim, J. Design Principle of Conjugated Polyelectrolytes to Make Them Water-Soluble and Highly Emissive. *Adv. Funct. Mater.* **2012**, *22*, 1076−1086.
(7) Duarte, A.; Pu, K. Y.; Liu, B.; Bazan, G. C. Recent Advances in Conjugated Polyelectrolytes for Emerging Optoelectronic Applications. *Chem. Mater.* **2011**, *23*, 501−515.
(8) Jenekhe, S. A.; Yi, S. Efficient Photovoltaic Cells from Semiconducting Polymer Heterojunctions. *Appl. Phys. Lett.* **2000**, *77*, 2635−2637.
(9) Kietzke, T.; Hoerhold, H. H.; Neher, D. Efficient Polymer Solar Cells Based on M3EH−PPV. *Chem. Mater.* **2005**, *17*, 6532−6537.
(10) Brabec, C. J.; Sariciftci, N. S.; Hummelen, J. C. Plastic Solar Cells. *Adv. Funct. Mater.* **2001**, *11*, 15−26.
(11) Gaylord, B. S.; Heeger, A. J.; Bazan, G. C. DNA Hybridization Detection with Water-Soluble Conjugated Polymers and Chromophore-Labeled Single-Stranded DNA. *J. Am. Chem. Soc.* **2003**, *125*, 896−900.
(12) Liu, B.; Bazan, G. C. Homogeneous Fluorescence-Based DNA Detection with Water-Soluble Conjugated Polymers. *Chem. Mater.* **2004**, *16*, 4467−4476.
(13) Tan, C.; Pinto, M. R.; Kose, M. E.; Ghiviriga, I.; Schanze, K. S. Solvent-Induced Self-Assembly of a Meta-Linked Conjugated Polyelectrolyte. Helix Formation, Guest Intercalation, and Amplified Quenching. *Adv. Mater.* **2004**, *16*, 1208−1212.
(14) Tan, C.; Pinto, M. R.; Schanze, K. S. Photophysics, Aggregation and Amplified Quenching of a Water-Soluble Poly(Phenylene Ethynylene). *Chem. Commun.* **2002**, *5*, 446−447.
(15) Tapia, M. J.; Burrows, H. D.; Valente, A. J. M.; Pradhan, S.; Scherf, U.; Lobo, M. M.; Pina, J.; Melo, J. S. Interaction between the Water Soluble Poly{1,4-phenylene-[9, 9-bis(4-phenoxy butylsulfonate)]fluorene-2,7-diyl} Copolymer and Ionic Surfactants Followed by Spectroscopic and Conductivity Measurements. *J. Phys. Chem. B* **2005**, *109*, 19108−19115.
(16) Sun, L. L.; Hao, D.; Zhang, P.; Qian, Z. S.; Shen, W. L.; Shao, T. L.; Zhu, C. Q. Indication of Critical Micelle Concentration of Nonionic Surfactants with Large Emission Change Using Water-soluble Conjugated Polymer as Molecular Light Switch. *J. Lumin.* **2013**, *134*, 260−265.
(17) Costa, T.; Garner, L. E.; Knaapila, M.; Thomas, A. W.; Rogers, S. E.; Bazan, G. C.; Burrows, H. D. Aggregation Properties of p-Phenylene Vinylene Based Conjugated Oligoelectrolytes with Surfactants. *Langmuir* **2013**, *29*, 10047−10058.
(18) Chen, L. H.; Xu, S.; McBranch, D.; Whitten, D. Tuning the Properties of Conjugated Polyelectrolytes through Surfactant Complexation. *J. Am. Chem. Soc.* **2000**, *122*, 9302−9303.
(19) Burrows, H. D.; Tapia, M. J.; Fonseca, S. M.; Pradhan, S.; Scherf, U.; Silva, C. L.; Pais, A. A. C. C.; Valente, A. J. M.; Schillén, K.; Alfredsson, V.; Carnerup, A. M.; Tomsic, M.; Jamnik, A. Solubilization of Poly{1,4-Phenylene-[9,9-Bis(4-Phenoxy-Butylsulfonate)]Fluorene-2,7-Diyl} in Water by Nonionic Amphiphiles. *Langmuir* **2009**, *25*, 5545−5556.
(20) Laurenti, M.; Rubio-Retama, J.; Garcia-Blanco, F.; Garcia-Blanco, F.; López-Cabarcos, E. Influence of the Surfactant Chain Length on the Fluorescence Properties of a Water-Soluble Conjugated Polymer. *Langmuir* **2008**, *24*, 13321−13327.
(21) Burrows, H. D.; Tapia, M. J.; Silva, C. L.; Pais, A. A. C. C.; Fonseca, S. M.; Pina, J.; Seixas de Melo, J.; Wang, Y. J.; Marques, E. F.; Knaapila, M.; Monkman, A. P.; Garamus, V. M.; Pradhan, S.; Scherf, U. Interplay of Electrostatic and Hydrophobic Effects with Binding of Cationic Gemini Surfactants and a Conjugated Polyanion: Experimental and Molecular Modeling Studies. *J. Phys. Chem. B* **2007**, *111*, 4401−4410.
(22) Menger, F. M.; Keiper, J. S. Gemini Surfactants. *Angew. Chem., Int. Ed.* **2000**, *39*, 1906−1920.
(23) Zana, R. Dimeric and Oligomeric Surfactants. Behavior at Interfaces and in Aqueous Solution: a Review. *Adv. Colloid Interface Sci.* **2002**, *97*, 205−253.
(24) Han, Y. C.; Wang, Y. L. Aggregation Behavior of Gemini Surfactants and Their Interaction with Macromolecules in Aqueous Solution. *Phys. Chem. Chem. Phys.* **2011**, *13*, 1939−1956.
(25) Wang, R. J.; Wang, Y. L. Interaction of Anionic Sulfonate Gemini Surfactant with PEO-PPO-PEO Triblock Copolymers. *Acta Chim. Sin.* **2014**, *72*, 41−50.
(26) Tang, Y. Q.; Wang, R. J.; Wang, Y. L. Constructing Gemini-Like Surfactants with Single-Chain Surfactant and Dicarboxylic Acid Sodium Salts. *J. Surfactants Deterg.* **2015**, *18*, 25−31.
(27) Yu, D. F.; Tian, M. Z.; Fan, Y. X.; Ji, G.; Wang, Y. L. Aggregate Transitions in Aqueous Solutions of Sodium Dodecylsulfate with a "Gemini-Type" Organic Salt. *J. Phys. Chem. B* **2012**, *116*, 6425−6430.
(28) Löffler, H.; Happle, R. Profile of Irritant Patch Testing with Detergents: Sodium Lauryl Sulfate, Sodium Laureth Sulfate and Alkyl Polyglucoside. *Contact Dermatitis* **2003**, *48*, 26−32.
(29) Turkoglu, M.; Sakr, A. Evaulation of Irritation Potential of Surfactant Mixtures. *Int. J. Cosmet. Sci.* **1999**, *21*, 371−382.
(30) Charbonnier, V.; Morrison, B. M., Jr.; Paye, M.; Maibach, H. I. Subclinical, Non-Erythematous Irritation with an Open Assay Model (Washing): Sodium Lauryl Sulfate (SLS) versus Sodium Laureth Sulfate (SLES). *Food Chem. Toxicol.* **2001**, *39*, 279−286.
(31) Ananthapadmanabhan, K. P.; Lips, A.; Vincent, C.; Meyer, F.; Caso, S.; Johnson, A.; Subramanyan, K.; Vethamuthu, M.; Rattinger, G.; Moore, D. J. pH-Induced Alterations in Stratum Corneum Properties. *Int. J. Cosmet. Sci.* **2003**, *25*, 103−112.
(32) Sharvelle, S.; Lattyak, R.; Banks, M. K. Evaluation of Biodegradability and Biodegradation Kinetics for Anionic, Nonionic, and Amphoteric Surfactants. *Water, Air Soil Poll.* **2007**, *183*, 177−186.
(33) Sibila, M. A.; Garrido, M. C.; Perales, J. A.; Quiroga, J. M. Ecotoxicity and Biodegradability of an Alkyl Ethoxysulphate Surfactant in Coastal Waters. *Sci. Total Environ.* **2008**, *394*, 265−274.
(34) Dhouib, A.; Hamad, N.; Hassaïri, I.; Sayadi, S. Degradation of Anionic Surfactants by *Citrobacter Braakii*. *Process Biochem.* **2003**, *38*, 1245−1250.
(35) Alargova, R. G.; Petkov, J. T.; Petsev, D. N. Micellization and Interfacial Properties of Alkyloxyethylene Sulfate Surfactants in the Presence of Multivalent Counterions. *J. Colloid Interface Sci.* **2003**, *261*, 1−11.
(36) Dahanayake, M.; Cohen, A. W.; Rosen, M. J. Relationship of Structure to Properties of Surfactants. 13. Surface and Thermodynamic Properties of Some Oxyethylenated Sulfates and Sulfonates. *J. Phys. Chem.* **1986**, *90*, 2413−2418.
(37) Aoudia, M.; Al-Maamari, T.; Al-Salmi, F. Intramolecular and Intermolecular Ion−dipole Interactions in Sodium Lauryl Ether Sulfates (SLES) Self-aggregation and Mixed Micellization with Triton X-100. *Colloids Surf., A* **2009**, *335*, 55−61.
(38) Aoudia, M.; Al-Haddabi, B.; Al-Harthi, Z.; Al-Rubkhi, A. Sodium Lauryl Ether Sulfate Micellization and Water Solubility Enhancement towards Naphthalene and Pyrene: Effect of the Degree of Ethoxylation. *J. Surfactants Deterg.* **2010**, *13*, 103−111.

DOI: 10.1021/la504733q
Langmuir 2015, 31, 2104−2111